Acta Ophthalmologica



# Simulation of specular microscopy images of corneal endothelium, a tool for control of measurement errors

Curry Bucht,[1,3] Per Söderberg[2] and Göran Manneberg[3]

[1]St. Erik's Eye Hospital, Karolinska Institutet, Stockholm, Sweden
[2]Gullstrand lab, Ophthalmology, Department of Neuroscience, Uppsala University, Uppsala, Sweden
[3]Biomedical Physics, Royal Institute of Technology, Stockholm, Sweden

## ABSTRACT

***Purpose:*** **We aimed at developing simulation software capable of producing images of corneal endothelium close to identical to images captured by clinical specular microscopy with defined morphometrical characteristics. It was further planned to demonstrate the usefulness of the simulator by analysing measurement errors associated with a trained operator using a commercially available semi-automatic algorithm for analysis of simulated images.**

***Methods:*** **Software was developed that allows creation of unique images of the corneal endothelium expressing morphology close to identical with that seen in images of corneal specular microscopy. Several hundred unique images of the corneal endothelium were generated with randomization, spanning a physiological range of endothelial cell density. As an example of the usefulness of the simulator for analysis of measurement errors in corneal specular microscopy, a total of 12 of all the images generated were randomly selected such that the endothelial cell density expressed was evenly distributed over the physiological range of endothelial cell density. The images were transferred to a personal computer. The imagenet-640 software was used to analyse endothelial cell size variation, percentage of hexagonal endothelial cells, and endothelial cell density.**

***Results:*** **The simulator developed allows randomized generation of corneal specular microscopy images with a preset expected average and variation of cell structure. Calculated morphometric information of each cell is stored in the simulator. The image quality can secondarily be varied with a toolbox of filters to approximate a large spectrum of clinically captured images. As an example of the use of the simulator, measurement errors associated with one trained operator using the imagenet-640 software, and focusing on endothelial cell density, were examined. The functional dependence between morphometric information estimated with the imagenet-640 software algorithm and real morphometric information as provided by the simulator was analysed with regression. It was demonstrated that that the estimations of endothelial cell size variation was associated with a scaling error and that the random error was strongly dependent on the operator.**

***Conclusion:*** **The newly developed simulator for randomized generation of morphometrically defined corneal specular microscopy images for the first time makes it possible to estimate a spatial scaling error of an available semi-automatic algorithm and to determine the random measurement error of important morphometric estimates in a defined reference sample of images. It is anticipated that the simulator will be a valuable tool for the generation of a large set of morphometrically well-characterized corneal specular microscopy images that can be used for calibration among research centres, for minimization of random errors and for measurement of quality control. Simulated images will be useful for the development of fully automatic analysis of corneal endothelial cell morphometry.**

**Key words:** cornea – density – endothelium – morphometry – pleomorphism – polymegethism – simulation

Acta Ophthalmol.


doi: 10.1111/j.1755-3768.2010.01974.x

## Introduction

The current paper describes a simulator for the generation of images of corneal endothelium as imaged with clinical specular microscopy (CSM).

The cornea serves as a protective barrier for the interior of the eye while simultaneously transmitting light. The cornea–air interface provides a large proportion of the refractive power of the optical apparatus of the eye because of a large shift of refractive index. High and even transmittance of the cornea is vital for clear vision. The innermost layer of the cornea, the endothelium, is a monolayer of flat, nonmitotic polygonal cells. In a healthy sample of corneal endothelium, a majority of the cells are hexagonal (Fig. 1).

The endothelium acts as a posterior physical barrier of the cornea and helps to control the fluid balance of the interior of the cornea by an energy-dependent mechanism. A well-functioning endothelium is vital for maintenance of the optical properties of the cornea. Surgical trauma to endothelial cells is repaired by lateral expansion of neighbouring endothelial cells, thus reducing the density of endothelial cells. If the density of endothelial cells becomes too low, the clarity of the cornea is threatened (Bourne et al. 1976; Waring et al. 1982). It is therefore important to evaluate the corneal endothelium prior to anterior segment surgery (Wirbelauer et al. 2005).

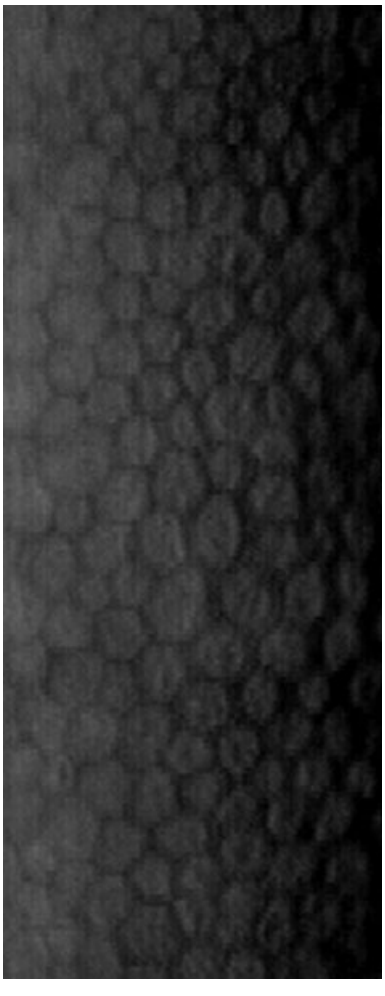

**Fig. 1.** Corneal endothelium imaged using clinical specular microscopy.

Morphometric variables of the corneal endothelium such as cell density, sometimes referred to as average cell size and cell size variation, usually expressed as coefficient of variation for cell size, are frequently analysed (Bursell et al. 1981; Lester et al. 1981; Schimmelpfennig 1984; Yee et al. 1985). Presently, morphometric variables of the corneal endothelium are most commonly estimated by CSM (Sturrock et al. 1978; Rao et al. 1982; Stur & Grabner 1983; Hartmann & Koditz 1984; Hirst et al. 1984; Glasser et al. 1985a,b; Hartmann et al. 1985; Matsuda et al. 1986; Siertsema et al. 1993). This technique can be tedious, and results are expected to vary because of field restriction and considerable spatial variability in the endothelium. The captured images undergo computerized enhancement. The morphometrical variables are calculated from the endothelial cell borders identified in the specular image. The detection of the cell borders requires time-consuming operator involvement in a majority of the cases (Cheung & Cho 2000; van Schaick et al. 2005). Variability in morphometric data among CSM systems and among operators and calibration differences between systems are also limiting factors for measurements (Landesz et al. 1995a,b; van Schaick et al. 2005; de Sanctis et al. 2006; Deb-Joardar et al. 2007a,b).

Because of the limitations of classic morphometric CSM analysis, new strategies are desirable. The periodic nature of the corneal endothelium makes morphometric analysis of its frequency domain an attractive alternative to the current CSM analysis. Epithelial cell analysis through Fraunhofer diffraction and thus an optical Fourier transform (Hecht 2002) was explored by Lambert and Klyce (Lambert & Klyce 1981) and was explored for analysis of corneal endothelium by Masters (Masters 1988; Masters et al. 1990). It has already been shown that the diffraction pattern of specular images of the corneal endothelium, obtained as the Fourier transform of the image, can be used to identify mean endothelial cell size and hence cell density (Doughty et al. 1997; Fitzke et al. 1997; Foracchia & Ruggeri 2004; Ruggeri et al. 2005, 2007).

However, no widely used working alternative method have been realized as of yet, and CSM with subsequent semi-automated border detection is still used for corneal endothelial morphometry. Development of an automized method would require an extensive reference database of clinically collected samples that is morphometrically characterized without significant random error. The lack of such a reference database has possibly been one important obstacle for transferring theoretical suggestions such as e.g. Fourier transforms of corneal endothelium to useful clinical strategies.

Current computer technology makes it possible to emulate images of morphometrically characterized cell structures. This provides a possibility to generate an extensive database of defined images by simulation. Such a database could be used for development of fully automatic algorithms for morphometry of the corneal endothelium.

There have been several attempts to develop algorithms for emulation of cell structure (Honda 1978; Weliky & Oster 1990; Meineke et al. 2001; Sanchez-Marin 2005). Simulation of cell structures has been shown as a useful tool to explore and evaluate new methods of cell morphometry (Fitzke et al. 1997; Bucht et al. 2006). Analysis of these studies revealed the need for a completely new simulator for clinical CSM images incorporating the following features: (i) The image should be generated based on randomization such that only the expected value and the variability of key independent morphometric variables are parameters for the randomization. (ii) The randomly generated cell structure should be morphometrically characterized without error. (iii) It should be possible to deteriorate the image quality with a set of filters to closely approximate image quality obtained when collecting images in a clinical setting.

The aim of the current study was to develop a software-based simulator based on the above three criteria. It was intended to use the simulator to generate a large database of morphometrically defined standard CSM images that can be used for validation of algorithms for morphometry of clinical CSM images. To demonstrate the realism of the CSM images automatically generated by the simulator and the simulator usefulness for evaluation of measurement errors associated with semi-automatic clinical CSM, it was planned to analyse measurement errors associated with a trained operator's estimation of polymegethism, pleomorphism and endothelial cell density in a subset of 12 images using the commercially available morphometric analysis software, IMAGNET-640 software.

# Materials and methods

### Simulation algorithm

The simulation software was developed in the mathematical programming language MATLAB (version 7.7.0; The Mathworks, Natick, MA, USA). The endothelium cell structure was created to represent a specular image in a two-dimensional matrix. This was developed in a few steps. Iterative trigonometric algorithms were used to

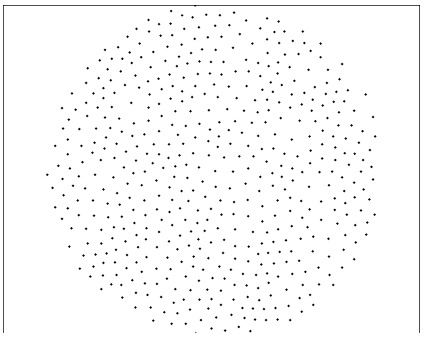

**Fig. 2.** Created cell co-ordinates of endothelial cells.

create a random pattern of cell co-ordinates (Fig. 2).

Each dot in Fig. 2 represents a cell in the endothelium, but not necessarily the centre of the cell. The authors are aware of possible exceptions in relative placement (Ikebe et al. 1986; Xie et al. 1991), but such exceptions were here omitted in the current algorithm.

The next step in the algorithm was to create cell barriers for the structure. A previous attempt on creating a endothelial cell simulator (Bucht et al. 2006) was based on the Voronoi geometrical method for creation of cell barriers. The approach using Voronoi, or Dirichlet tessellation for simulation of cells was introduced by Honda (Honda 1978) and followed up by Weliky et al. (Weliky & Oster 1990) and Meineke (Meineke et al. 2001). Simulation of corneal endothelium using Voronoi was also performed by Sanchez-Marin (Sanchez-Marin 2005).

In the current version of the cell simulator, it was considered imperative to know exactly which barrier belonged to which cell. A new algorithm similar but not identical to the Voronoi geometrical method was used. The vertices making for every cell corner co-ordinate were created by finding the centroid of the three cells sharing the corner. Each cell corner was associated with its corresponding cell. The cell barriers were then made up from the line segments connecting all cell corner vertices around the cell. In this way, full knowledge on which cell corner that belong to which cell was gained and stored for later use.

Once the cell corner vertex co-ordinates were created, realistic cell barrier graphics were created and drawn in the two-dimensional matrix (Fig. 3). In CSM imaging, light impinges on the cell structure from an angle. Because of this, cell barrier image contrast is angle dependent. This was accounted for in the barrier graphics algorithm, and the visual effect of varying angles of impinging light was introduced as an option in the software.

The next step in the CSM image simulation was to extract an area and a cell density of the simulated cell structure equal to that of a typical CSM image (Fig. 4, left).

In the present study, we aimed at using simulated images for the determination of the accuracy of barrier tracing morphometry. Morphological data accompanying each simulated CSM image were limited to cells completely inside the image (Fig. 4, right). Morphological data of cells bordering the CSM image area was omitted by choice, because of that these cells are not accounted for in border trace morphometry.

After extracting a cell structure corresponding to clinically relevant CSM image shape and cell density, numerous filters were created and applied to simulate real CSM image appearance. Noise, illumination profiles and contrast were all made variable parameters in the software. None of the filters used introduced any systematic lateral change in the image and even though the quality of the image would be degraded, morphometric characteristics were not systematically effected (Fig. 5).

In Fig. 5, three typical CSM image qualities are displayed. The leftmost image shows an even and desired contrast and illumination. The middle image gives an example of a typical varying contrast image. The rightmost image in Fig. 5 shows an example of a CSM image of the endothelium with varying illumination. The filter functionality was anticipated to be valuable in future use of the simulator e.g. for development of new automated methods for corneal endothelium morphometry.

The number of corneal endothelial cells and numbers of corners corresponding to each cell are known parameters in the simulation algorithm. From this, the percentage of hexagonal cells is thus given. Any polygon can be broken down into a set of triangles. The area of each cell was calculated by area triangulation (Heron's formula) and successive addition of the triangulated areas. For a hexagon, four triangles are added (Fig. 6), but the method holds for any polygonal shape.

Corneal endothelial cell density as well as coefficient of variation of cell size or any other morphometric variable could therefore easily be calculated for each simulated CSM image.

### Simulation and estimating measurement errors in morphometry in CSM images

Altogether, 500 unique images of the corneal endothelium were simulated. All images came with known morphological data, showing coefficient of variation of cell sizes (polymegethism), percentage of hexagonal cells (pleomorphism) and cell density. The 500 images spanned a clinical range from low to high cell densities. All images were of good quality, aiming at facilitating the operator-guided barrier tracing.

As an example of how the simulated images can be used for estimation of measurement errors, a total of 12 of the 500 images were chosen for semi-automated barrier trace morphometry with focus on corneal cell density performed by one operator. The 12 images were selected to represent a physiological range of corneal cell density and image quality. The

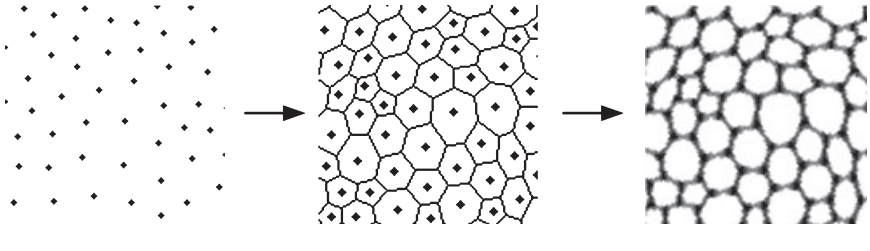

**Fig. 3.** Generation of cells from cell centroids (left), through schematic bordered cells (middle) to final bordered cells (right).

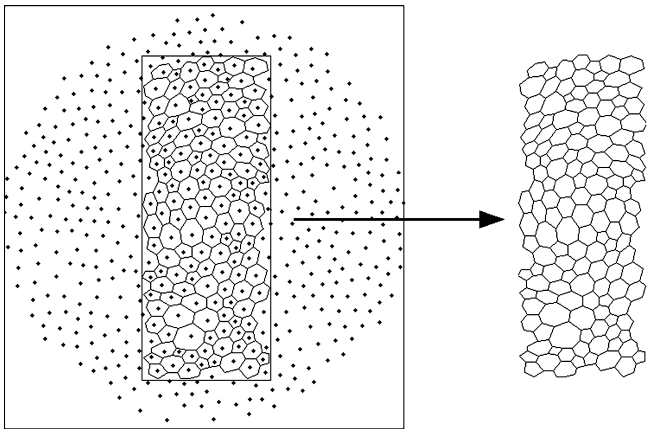

**Fig. 4.** Schematic of endothelial cells generated. *Left:* Area of interest, matching that of a typical clinical specular microscopy image. *Right:* All cells completely inside the relevant area of analysis.

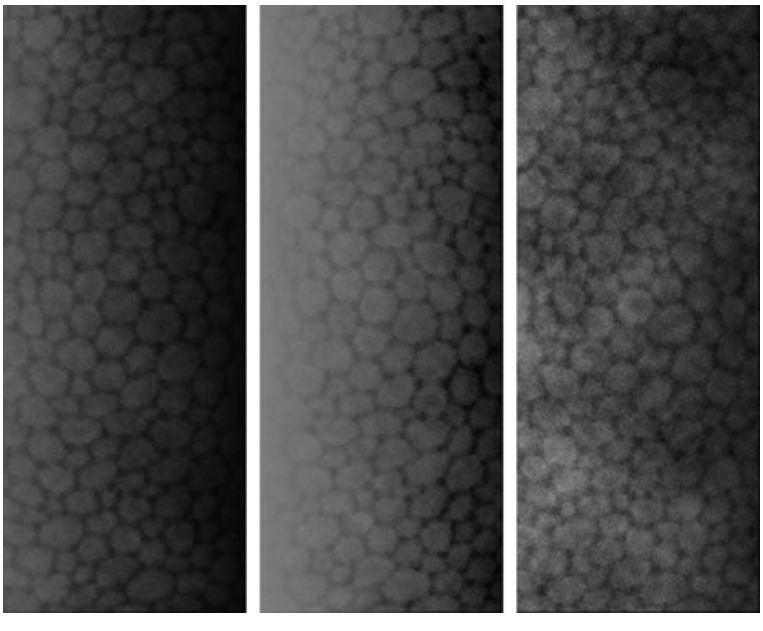

**Fig. 5.** One simulated clinical specular microscopy image filtered 3 times, showing possibilities of varying image quality for a defined sample of cells with defined morphometric characteristics.

lower density limit corresponding to what is normally considered the lower limit for donor cornea endothelial cell density (Schroeter & Rieck 2009) and the total range with some margin within a practical physiological range of cell densities of the corneal endothelium (Wiffen et al. 1995). The number of cells per image ranged from 132 to 266 (Fig. 7).

The 12 simulated CSM images were all formatted to match the size and compression of real corneal endothelium images captured by the TOPCON CSM and stored in the IMAGENET-640 software. In this way, simulated images could replace real images in the PC for analysis with the semi-automated barrier tracing morphometry software. Each of the 12 simulated images underwent semi-automated barrier tracing analysis, one at a time. The simulated image was loaded into the IMAGENET-640 software. The operator then chose the area of the image to be analysed. The complete areas of all images were chosen. In the next step, IMAGENET-640 automatically enhances the contrast and light distribution of the image, making it more susceptible to barrier tracing. When image quality was optimized, an automated attempt on tracing the cell barriers began. The

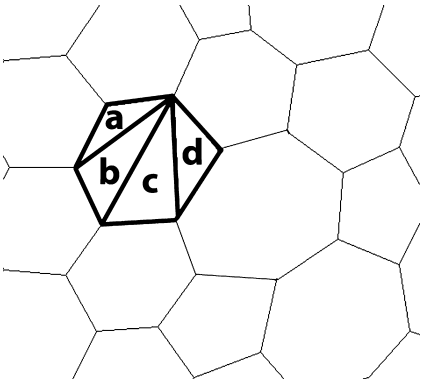


**Fig. 6.** Calculating the area of each individual cell by addition of triangulated areas a, b, c and d.

automated barrier trace did not succeed to a sufficient extent, and all images therefore had to undergo manual correction by the operator.

The human factor plays a noticeable role in the process of semi-automated corneal endothelial barrier tracing analysis, because as stated, the computer will generally not trace the exact cell barriers. The manual barrier retracing of erroneous computerized cell barrier tracing was conducted by the operator without prior knowledge of the cell density of the simulated image and in a random order. In the present study, cell density was prioritized. During manual retracing, it was attempted to identify the borders of the cells that had been simulated. Special attention was focused on the fact that the barrier trace software did not analyse 'split' or 'multiple' cells, as this would introduce a cell count error and thus erroneous corneal endothelial cell density estimation (Fig. 8).

When all 12 images had been analysed using the barrier tracing software, the scale of the stored relative information on individual geometry of each cell was adjusted so that the average cell density for the simulated images was equal to the average cell density estimated with the barrier tracing software. On an absolute scale, the cell densities of the 12 images were found to be linearly spaced from 1994 to 3907 cells/mm$^2$, corresponding to 132–266 cells per image, respectively (Fig. 7).

### Statistics

The confidence coefficient was set to 95% considering the sample size.

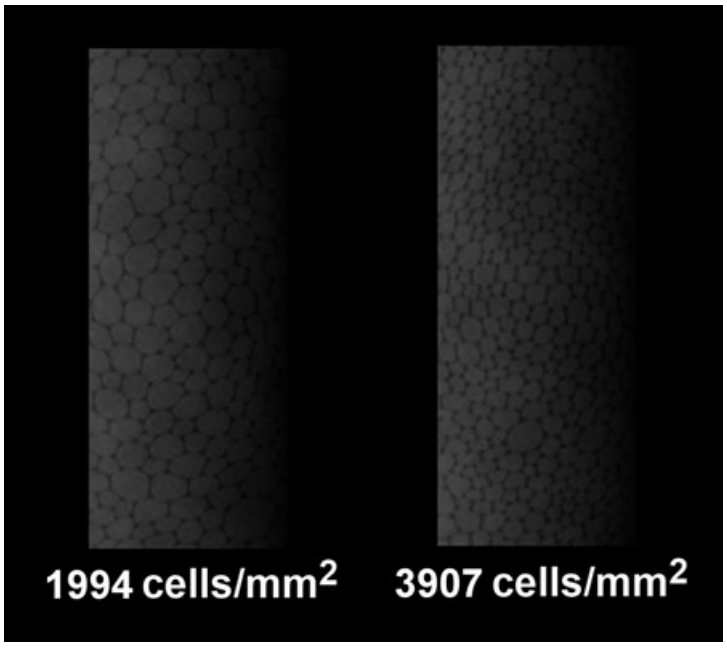


**Fig. 7.** The two endothelial cell density extremes of the 12 images used for semi-automated barrier tracing morphometry.

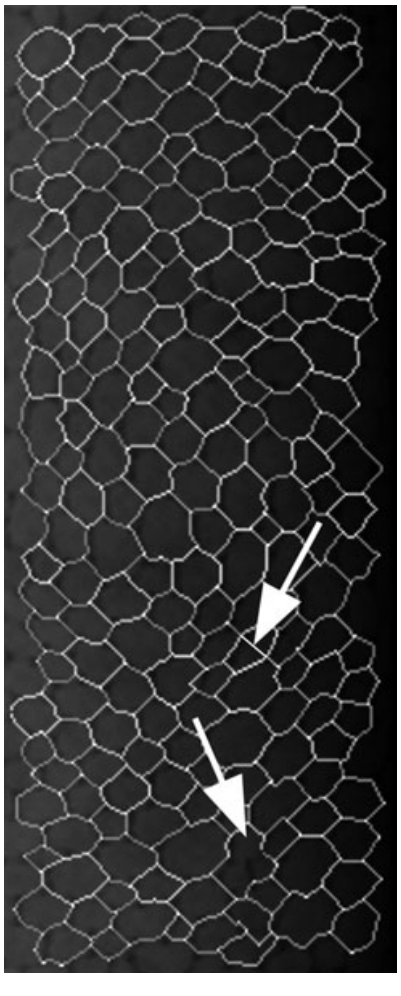

**Fig. 8.** Barrier tracing of simulated corneal endothelium. *Upper arrow:* A split cell counted as two. *Lower arrow:* Multiple cells, counted as one.

# Results

### The simulator

The development of software for simulation of images of the corneal endothelium captured by specular microscopy was completed. The simulator meets the requirements stipulated: (i) The image is based on randomization guided by a possibility to preset average and variability of the final cell structure. (ii) The morphometric characteristics of the simulated cell structure are calculated and stored. (iii) Image quality can be secondarily altered by a set of filters to approximate a large spectrum of clinically captured images.

The process of creating and storing an arbitrary amount of unique images of the corneal endothelium is fully automated. The creation of each complete CSM image, including application of filters for variation of image quality, took approximately 20 seconds on a standard personal computer. The simulation time could easily be substantially reduced by optimizing the software and using a faster computer.

### Semi-automated analysis of simulator-generated corneal endothelial images by a trained operator

The average analysis time for one image using the operator-dependent semi-automatic barrier tracing method was approximately 10 min. The operator-dependent semi-automatic barrier tracing method provided, for each simulated picture, estimates of coefficient of variation of cell size, *polymegethism*, proportion of hexagonality, *pleomorphism* and corneal endothelial cell density. For each of these variables, the estimates were compared to the real values as provided by the simulator that generated the images, and the errors in the semi-automatic operator-dependent measure were estimated.

To compare estimated morphometric information as obtained by the semi-automatic morphometric analysis with real morphometric information as provided by the simulator, the estimated morphometric information for each image was plotted as a function of the real morphometric information for each of the morphometric variables, after transformation in accordance with Appendix 1 (Fig. 9).

For each morphometric variable, a potential scaling error in the semi-automatic algorithm was examined as an estimated 95 % confidence interval for the inclination coefficient obtained from the regression (Table 1 – 2nd column).

The precision of the estimate was estimated as a 95 % confidence interval for the residual standard deviation obtained from the regression (Table 1 – 3rd column).

It was found that for the well-trained operator estimation of polymegethism was associated with a scaling error (Table 1, polymegethism, 2nd column) as indicated by the fact that the confidence interval for the inclination coefficient excluded 1.

The operator, in the interest of analysis time, was focusing on correcting missing cell barriers during the morphometric analysis rather than adjusting each corner of the cells under investigation. The present analysis of the precision of the estimates (Table 1, 5th column) demonstrates that that strategy is associated with considerable random error in the estimate of polymegethism but provides a low randow error in estimates of cell density.

# Discussion

In the current study, we developed a simulator that can generate images of corneal endothelial cells as obtained

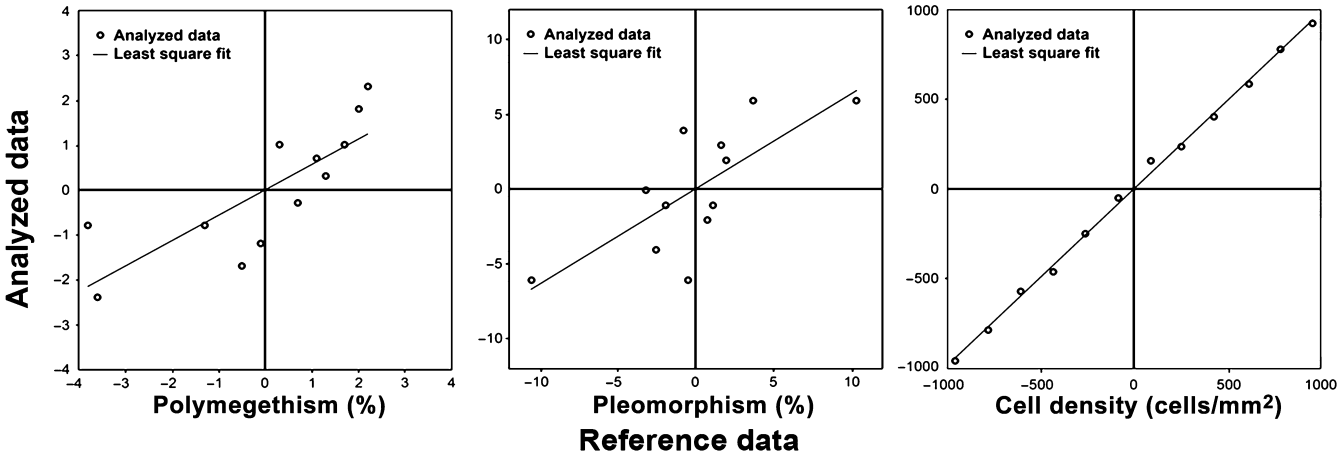


**Fig. 9.** Estimated reduced polymegethism (left), pleomorphism (middle) and endothelial cell density (right) as a function of reduced reference data. Straight line is best-fit least-square regression.

**Table 1.** Measurements errors in semi-automatic morphometric analysis for a well-trained operator focusing on correcting missing cell barriers as identified by the semi-automatic algorithm.

| | | Precision | | |
|---|---|---|---|---|
| Morphometric variable | Scaling error 95% confidence interval for inclination coefficient* (unitless) | 95 % confidence interval for residual standard deviation* | Estimated average level in sample | Corresponding variation coefficient Residual standard deviation/average estimated level (unitless) |
| Polymegethism (Variation coefficient for cell size) | 0.57 ± 0.39† | [0.6; 1.5] unitless | 0.414 unitless | [1.5–3.6] |
| Pleomorphism (Proportion of hexagonality) | 0.63 ± 0.39 | [2.0; 4.9]% | 44.1% | [0.05–0.11] |
| Endothelial cell density | 0.98 ± 0.03 | [20.9; 50.1] cells/mm$^2$ | 2 951 cells/mm$^2$ | [0.007–0.017] |

* Degrees of freedom = 11.
† Significant deviation from 1.

by CSM. The simulator provides known reference morphometric descriptors of all the simulated cells in each image. One trained operator analysed simulated images with the operator-dependent semi-automatic algorithm provided with a commercially available specular microscope without prior knowledge of the morphometric characteristics of the simulated images. This allowed estimation of measurement errors of the semi-automatic method associated with a trained operator.

### The simulator

The purpose of the first part of the present study was to develop software capable of mimicking real images of corneal endothelium, as captured by CSM. The main future use of the simulator is anticipated to be on-demand generation of databases containing a large amount of morphometrically defined images of corneal endothelium. Considering our purpose, the process of rendering and storing images as well as their corresponding morphological variables had to be fully automated.

The current simulator is a further development of previously published work on emulation of cell structure (Honda 1978; Weliky & Oster 1990; Fitzke et al. 1997; Meineke et al. 2001; Sanchez-Marin 2005; Bucht et al. 2006). The algorithm in the current study is in every part a new development but based on experience gathered from application of previously published algorithms. We here included generation of the cell structure by automated randomization with fully defined resulting cell morphometry parameters for each individual cell in each image simulated. This is necessary to simulate realistic unbiased images. The randomization makes it impossible to set exact morphometric characteristics of an image before it has been created. It is only possible to preset the mean level of the cell density and the variation of cell size, respectively. Pleomorphism and polymegethism are related in the simulator as are they in real-life corneal endothelium (Doughty 1998). The problem of not knowing beforehand the exact outcome of morphometric parameters because of the randomization is made up for by the ability to automatically create literally thousands of images, and each image is, once generated with randomization, calculated for morphometrical characteristics. Thus, a subset of generated images with specified morphometric characteristics can secondarily be selected for any strategy for specific morphometric analysis.

Every individual cell in the structure is created and handled through a fully controlled algorithm. Thereby, not only the number of cells created and their mean size is known in the simulator, but also the area and number of corners of each unique cell are known and stored in the simulator. This

allows extraction of segments of a larger cell structure with retained morphometric information about the cells in the segment extracted, even if the morphology of the bigger structure varies.

The fact that an option exists to secondarily vary the quality of the simulated image in the simulator with filters for light profiles, noise and contrast makes it possible to create realistic images. This is anticipated to be a useful feature to establish the robustness of semi-automatic and automatic algorithms for morphometric cell analysis.

Image sizes of the samples and thus the area of the endothelium in the limited example study were fixed. As the number of cells within the image area is squared proportional to the length of the image border, cell density estimation is anticipated to become more accurate with larger image samples.

**Semi-automatic estimation of morphometric information in simulator-generated images**

All semi-automatic strategies for morphometry are associated with errors, partly related to relative capacity of the cell border detection software to correctly identify cell borders and partly related to the relative attention of the operator to correct the automatic cell border detection. The currently used software for semi-automatic morphometric analysis, IMAGENET-640 software, is based on cell barrier tracing for analysis. Another widely used method is the cell centre dot method, which was not used in this study. For corneal cell density estimates, the two methods perform equally well, while the barrier trace method is more reliable for the estimation of polymegethism and pleomorphism (Deb-Joardar et al. 2007b).

Estimation of morphometric information from CSM images requires calibration of the level of the linear scale, calibration of the sensitivity over the range in focus and minimization of the random error by appropriate experimental design.

In the present study, the measurement errors associated with one trained operator were analysed as an example of how the simulator can be used. A complete analysis of the precision in estimates with semi-automatic algorithms and related potential sources of variation in measurements for any random operator is beyond the scope of the current paper.

The range of cell densities chosen for the analysis corresponds to the range found in normal corneas with the lower density limit corresponding to what is generally considered the lower limit in donor corneal endothelial cell density (Schroeter & Rieck 2009). The impact of extreme low or high cell density on the precision in estimates of morphometric variables is a specific question that should be addressed in a separate research project.

The number of independent images presently analysed was chosen considering the fact that according to the t-distribution, little further precision is achieved in estimates of parameters by increasing the sample size beyond 12.

*Calibration of the level of the linear scale*

In the present study, we calibrated the spatial scale of the simulated images to the average reading provided by semi-automated algorithm. Thus, the scale level is a priori correctly calibrated in level with the semi-automatic algorithm, but not necessarily with reality.

*Calibration of the sensitivity over the range in focus*

The currently developed simulator allows objective calibration of the sensitivity of any CSM instrument. In the present study we, by adopting Eqn 4, Appendix 1 assumed that, if any, there is a constant proportionality error for spatial measures of cell density, cell size coefficient of variation and hexagonality in the semi-automated algorithm within the measurement range. A potential constant proportionality error has previously not been possible to estimate because of lack of fully objective information on the morphometric characteristics of the reference sample. The fact that the experimental observations randomly distributes around the regression line (Fig. 9) suggests that it is sufficient to assume a potential constant proportionality error in sensitivity.

The reducing transform adopted (Appendix 1) allowed estimation of the scaling error without impact of the absolute level of the measurements.

*Standard for calibration of CSM measurements*

The random error in morphometric measurements of corneal endothelium originates from several potential sources of variation. A common model for analysing the random error in endothelial morphometry is to divide the random error into inter-system variation, inter-operator variation and measurement error. Inter-system variation, which involves inter-operator variation, has been analysed in several recent studies (Deb-Joardar et al. 2007a,b; Hirneiss et al. 2007; Doughty & Oblak 2008). Such estimates, unfortunately, are limited to repeated measurements by a number of operators on the same defined clinical material and therefore are limited to that specific clinical material. Inter-individual measurement error of the algorithm for a known standard set of images has previously not been possible to study, because of lack of a known standard set of images.

In the current study, the reference population, the standard set of images, is objectively defined with regard to coefficient of variation of cell size and proportion of hexagonality, and corneal endothelium cell density. We therefore for the first time were able to determine the inter-individual random measurement error in the semi-automatic algorithm for a standard set of images.

*Measurement errors associated with the trained operator in the present study*

The fact that the confidence interval for the inclination coefficient for estimated polymegethism excluded 1 (Fig. 9 – left panel, Table 1 – 2nd column) indicates that for that operator a correction factor should have been applied in a clinical setting to reduce the measurement error in estimates of polymegethism. For pleomorphism (Fig. 9 – middle panel, Table 1 – 2nd column), it was not possible to resolve a potential scaling error possibly because of the large random error in relation to the absolute level Table 1 – 5th column. Correction, therefore, would not decrease the measurement error if single semi-automatic estimates are adopted. This example demonstrates how it is possible to use the

simulator to monitor a potential operator, e.g. at regular intervals, and based on the outcome, associate a personal correction factor for the operator.

In the current study, the precision estimated as the ratio between the residual standard deviation and the average estimated level (Table 1, 5th column) for polymegethism and pleomorphism was consistent with findings in other studies where inter-operator and inter-system variances were examined (de Sanctis et al. 2006; Deb-Joardar et al. 2007a,b). In the current study, the operator focused attention on cell density measurement. The operator who performed the barrier tracing for the semi-automated barrier measurements therefore put limited attention on exactly tracing the corners of each cell, other than correcting clearly off-size cells. A comparison of the estimated random variation for the various morphometric variables analysed (Table 1, 5th column) demonstrates that operator attention is critical for the resulting magnitude of the random measurement error. Low attention on correcting the corners provides a significantly larger random error in the estimates of polymegethism and pleomorphism than the estimate of cell density. This confirms recent similar findings (Oblak et al. 2002; Sheng et al. 2007; Doughty 2008; Doughty & Aakre 2008; Doughty & Oblak 2008).

The estimated residual standard deviations, $s_{x/y}$ (Table 1, 3rd column) are random errors associated with single estimates of each image. The precision could be improved by averaging over several independent measurements of the same image. The random error as a function of the number of independent estimates of each image, $s(n)$, would then simply be a function of the number of independent estimates of the same image (Eqn 1).

$$s(n) = \sqrt{\frac{s_{x/y}^2}{n}} \qquad (1)$$

The low residual standard deviation found for estimates of corneal endothelial cell density (Fig. 9 – right panel, Table 1 – 3rd and 5th column) is the true variability of measurements caused by the semi-automated barrier tracing method used by the current operator as the reference data is known. Inter-operator and inter-system studies typically result in higher variations (de Sanctis et al. 2006; Deb-Joardar et al. 2007a,b) associated with variabilities among systems and operators. Such variabilities could be analysed with a standardize strategy based on a standard set of images generated with the currently developed simulator, but such analysis is beyond the scope of the present project.

## Acknowledgements

This study was supported by Karolinska Institutet Research Foundation, Swedish Research Council, projects K2006-74X-15035-03-2 and K2008-63X-15035-05-2, Carmen och Bertil Regnérs fond för forskning, Synfrämjandets forskningsfond, ELFA's forskningsstiftelse, Stockholms läns landsting research grants (FoUU), KI-KID grant.

## References

Bourne WM, McCarey BE & Kaufman HE (1976): Specular microscopy of human corneal endothelium in vivo. Am J Ophthalmol **81**: 319–323.

Bucht C, Söderberg PG & Manneberg G (2006): A model for corneal endothelial morphometry by diffraction. SPIE Proc **6138**: O1–O8.

Bursell SE, Hultgren BH & Laing RA (1981): Evaluation of the corneal endothelial mosaic using an analysis of nearest nieghbor distances. Exp Eye Res **32**: 31–38.

Cheung SW & Cho P (2000): Endothelial cells analysis with the TOPCON specular microscope SP-2000P and IMAGEnet system. Curr Eye Res **21**: 788–798.

Deb-Joardar N, Thuret G, Gavet Y, Acquart S, Garraud O, Egelhoffer H & Gain P (2007a): Reproducibility of endothelial assessment during corneal organ culture: comparison of a computer-assisted analyzer with manual methods. Invest Ophthalmol Vis Sci **48**: 2062–2067.

Deb-Joardar N, Thuret G, Zhao M, Acquart S, Peoc'h M, Garraud O & Gain P (2007b): Comparison of two semiautomated methods for evaluating endothelial cells of eye bank corneas. Invest Ophthalmol Vis Sci **48**: 3077–3082.

Doughty MJ (1998): Prevalence of 'non-hexagonal' cells in the corneal endothelium of young Caucasian adults, and their interrelationships. Ophthalmic Physiol Opt **18**: 415–422.

Doughty MJ (2008): Could the coefficient of variation (COV) of the corneal endothelium be overestimated when a centre-dot method is used? Clin Exp Optom **91**: 103–110.

Doughty MJ & Aakre BM (2008): Further analysis of assessments of the coefficient of variation of corneal endothelial cell areas from specular microscopic images. Clin Exp Optom **91**: 438–446.

Doughty MJ & Oblak E (2008): A comparison of two methods for estimating polymegethism in cell areas of the human corneal endothelium. Ophthalmic Physiol Opt **28**: 47–56.

Doughty MJ, Spiteri M & Dilts DM (1997): Determination of the unit size of the corneal endothelial cell mosaic from Fourier component image analysis. Tissue Cell **29**: 229–238.

Fitzke FW, Masters BR, Buckley RJ & Speedwell L (1997): Fourier transform analysis of human corneal endothelial specular photomicrographs. Exp Eye Res **65**: 205–214.

Foracchia M & Ruggeri A (2004): Automatic estimation of endothelium cell density in donor corneas by means of Fourier analysis. Med Biol Eng Comput **42**: 725–731.

Glasser DB, Matsuda M, Ellis JG & Edelhauser HF (1985a): Corneal endothelial morphology after anterior chamber lens implantation. Arch Ophthalmol **103**: 1347–1349.

Glasser DB, Matsuda M, Ellis JG & Edelhauser HF (1985b): Effects of intraocular irrigation solutions on the corneal endothelium after in vivo anterior chamber irrigation. Am J Ophthalmol **1985**: 321–328.

Hartmann C & Koditz W (1984): Automated morphometric endothelial analysis combined with video specular microscopy. Cornea **3**: 155–167.

Hartmann C, Kolb M, Knauer I & Konen W (1985): Clinical specular microscopy. Technic, organization and simple calculator morphometry. Klin Monatsbl Augenheilkd **186**: 96–104.

Hecht E (2002): Optics – International Edition. San Francisco, CA: Addison Wesley 452–457, 519–524.

Hirneiss C, Schumann RG, Gruterich M, Welge-Luessen UC, Kampik A & Neubauer AS (2007): Endothelial cell density in donor corneas: a comparison of automatic software programs with manual counting. Cornea **26**: 80–83.

Hirst LW, Sterner RE & Grant DG (1984): Automated analysis of wide-field specular photomicrographs. Cornea **3**: 83–87.

Honda H (1978): Description of cellular patterns by Dirichlet domains: the two-dimenstional case. J Theor Biol **72**: 523–543.

Ikebe H, Takamatsu T, Itoi M & Fujita S (1986): Age-dependent changes in nuclear DNA content and cell size of presumably normal human corneal endothelium. Exp Eye Res **43**: 251–258.

Lambert SR & Klyce SD (1981): The origins of Sattler's veil. Am J Ophthalmol **91**: 51–56.

Landesz M, Kamps A, Slart R, Siertsema JV & van Rij G (1995a): Morphometric analysis of the corneal endothelium with three different specular microscopes. Doc Ophthalmol **90**: 15–28.

Landesz M, Siertsema JV & Van Rij G (1995b): Comparative study of three semi-automated specular microscopes. J Cataract Refract Surg **21**: 409–416.

Lester JM, McFarland JL, Bursell SE, Laing RA & Brenner JF (1981): Automated morphometric analysis of corneal endothelial cells. Invest Ophthalmol Vis Sci **20**: 407–410.

Masters BR (1988): Characterisation of corneal specular endothelial photomicrographs by their Fourier transforms. SPIE Proc **938**: 246–252.

Masters BR, Lee YK & Rhodes WT (1990): Noninvasive diagnostic techniques in ophtalmology. New York: Springer-Verlag 122.

Matsuda M, Yee RW, Glasser DB, Geroski DH & Edelhauser HF (1986): Specular microscopic evaluation of donor corneal endothelium. Arch Ophthalmol **104**: 259–262.

Meineke FA, Potten CS & Loeffer M (2001): Cell migration and organization in the intestinal crypt using a latice-free model. Cell Prolif **34**: 253–266.

Oblak E, Doughty MJ & Oblak L (2002): A semi-automated assessment of cell size and shape in monolayers, with optional adjustment for the cell-cell border width-application to human corneal endothelium. Tissue Cell **34**: 283–295.

Rao GN, Lohman LE & Aquavella JV (1982): Cell size-shape relationships in corneal endothelium. Invest Ophthalmol Vis Sci **22**: 271–274.

Ruggeri A, Grisan E & Jaroszewski J (2005): A new system for the automatic estimation of endothelial cell density in donor corneas. Br J Ophthalmol **89**: 306–311.

Ruggeri A, Grisan E & Schroeter J (2007): Evaluation of repeatability for the automatic estimation of endothelial cell density in donor corneas. Br J Ophthalmol **91**: 1213–1215.

Sanchez-Marin FJ (2005): A simple procedure for simulating samples of tissue using voronoi diagrams. Anal Quant Cytol Histol **27**: 225–231.

de Sanctis U, Machetta F, Razzano L, Dalmasso P & Grignolo FM (2006): Corneal endothelium evaluation with 2 noncontact specular microscopes and their semiautomated methods of analysis. Cornea **25**: 501–506.

van Schaick W, van Dooren BT, Mulder PG & Volker-Dieben HJ (2005): Validity of endothelial cell analysis methods and recommendations for calibration in Topcon SP-2000P specular microscopy. Cornea **24**: 538–544.

Schimmelpfennig BH (1984): Direct and indirect determination of nonuniform cell density distribution in human corneal endothelium. Invest Ophthalmol Vis Sci **25**: 223–229.

Schroeter J & Rieck P (2009): Endothelial evaluation in the cornea bank. Dev Ophthalmol **43**: 47–62.

Sheng H, Parker EJ & Bullimore MA (2007): An evaluation of the ConfoScan3 for corneal endothelial morphology analysis. Optom Vis Sci **84**: 888–895.

Siertsema JV, Landesz M, van den Brom H & van Rij G (1993): Automated video image morphometry of the corneal endothelium. Doc Ophthalmol **85**: 35–44.

Stur M & Grabner G (1983): The corneal endothelium–morphology, function and clinical importance. Wien Klin Wochenschr **95**: 274–276.

Sturrock GD, Sherrard ES & Rice NSC (1978): Specular microscopy of the corneal endothelium. Br J Ophthalmol **62**: 809–814.

Waring GO III, Bourne WM, Edelhauser HF & Kenyon KR (1982): The corneal endothelium. Normal and pathologic structure and function. Ophthalmology **89**: 531–590.

Weliky M & Oster G (1990): The mechanical basis of cell rearrangement. I. Epithelial morphogenesis during Fundulus epiboly. Development **109**: 373–386.

Wiffen SJ, Nelson LR, Ali AF & Bourne WM (1995): Morphologic assessment of corneal endothelium by specular microscopy in evaluation of donor corneas for transplantation. Cornea **14**: 554–561.

Wirbelauer C, Wollensak G & Pham DT (2005): Influence of cataract surgery on corneal endothelial cell density estimation. Cornea **24**: 135–140.

Xie Q, Xiangming G & Miaorong S (1991): Dynamics of endothelial cells of the peripheral area of cornea. Yan Ke Xue Bao **7**: 63–66.

Yee RW, Matsuda M, Schultz RO & Edelhauser HF (1985): Changes in the normal corneal endothelial cellular pattern as a function of age. Curr Eye Res **4**: 671–678.

Received on November 17th, 2009.
Accepted on June 13th, 2010.

*Correspondence:*
Curry Bucht,
Research Department,
St. Erik's Eye Hospital
Karolinska Institutet
Polhemsgatan 50
SE-112 82 Stockholm
Sweden
Tel: + 46 8 6723511
Fax: + 46 8 672 3352
Email: curry.bucht@ste.ki.se

# Appendix 1

### Strategy for estimating errors in the semi-automatic operator-dependent measure

On the condition that the scaling of the semi-automatic operator-dependent measures is constant, a plot of operator-dependent semi-automatic estimated values, $s_i$, as a function of the corresponding calculated reference values, $r_i$, obtained from the simulator, for the ith image, is expected to reveal scattered points around an average straight line. If all estimated operator-dependent semi-automatic values are reduced with the average operator-dependent semi-automatic value, $\bar{s_i}$, $s_i'$ (Eqn 2).

$$s_i' = s_i - \bar{s_i} \tag{2}$$

and simultaneously all reference values are reduced with the average reference value, $\bar{r_i}$, $r_i'$ (Eqn 3).

$$r_i' = r_i - \bar{r_i} \tag{3}$$

and $s_i'$ is plotted as a function of $r_i'$, the plot is expected to reveal scattered points around an average straight line that intersects with the origin. The deviations from the straight line along the y-axis is a measure of the random error in the semi-automatic operator-dependent measurement, $\varepsilon_i$. The relationship between $s_i'$ and $r_i'$ then can be modelled as a straight line through the origin (Eqn 4).

$$s_i' = k \cdot r_i' + \varepsilon_i \tag{4}$$

If the data are analysed with regression assuming Eqn 4, the inclination coefficient, $k$, and the random error, $\sigma_\varepsilon$, can be estimated as a confidence interval. As the scale of the calculated reference values is known to be correct, any deviation of the regression coefficient, $k$, from one would indicate a constant scale error in the algorithm for semi-automatic operator measure.